Structural Engineering and Mechanics, *Vol. 73, No. 3 (2020) 239-257*
DOI: https://doi.org/10.12989/sem.2020.73.3.239

Novel steel bracket and haunch hybrid system for post-earthquake retrofit of damaged exterior beam-column sub-assemblages

A. Kanchanadevi*[1,2] and K. Ramanjaneyulu[1,2a]

[1]*CSIR-Structural Engineering Research Centre, Chennai, Tamil Nadu, India*
[2]*Academy of Scientific and Innovative Research (AcSIR), India*

(Received May 16, 2019, Revised August 18, 2019, Accepted October 5, 2019)

Abstract. In the present study, an innovative steel bracket and haunch hybrid scheme is devised, for retrofitting of earthquake damaged deficient beam-column sub-assemblages. Formulations are presented for evaluating haunch force factor under combined load case of lateral and gravity loads for the design of double haunch retrofit. The strength hierarchies of control and retrofitted beam-column sub-assemblages are established to showcase the efficacy of the retrofit in reversing the undesirable strength hierarchy. Further, the efficacy of the proposed retrofit scheme is demonstrated through experimental investigations carried out on gravity load designed (GLD), non-ductile and ductile detailed beam-column sub-assemblages which were damaged under reverse cyclic loading. The maximum load carried by repaired and retrofitted GLD specimen in positive and negative cycle is 12% and 28% respectively higher than that of the control GLD specimen. Further, the retrofitted GLD specimen sustained load up to drift ratio of 5.88% compared with 2.94% drift sustained by control GLD specimen. Repaired and retrofitted non-ductile specimen, could attain the displacement ductility of three during positive cycle of loading and showed improved ductility well above the expected displacement ductility of three during negative cycle. The hybrid haunch retrofit restored the load carrying capacity of damaged ductile specimen to the original level of control specimen and improved the ductility closer to the expected displacement ductility of five. The total cumulative energy dissipated by repaired and retrofitted GLD, non-ductile and ductile specimens are respectively 6.5 times, 2.31 times, 1.21 times that of the corresponding undamaged control specimens. Further, the damage indices of the repaired and retrofitted specimens are found to be lower than that of the corresponding control specimens. The novel and innovative steel bracket and haunch hybrid retrofit scheme proposed in the present study demonstrated its effectiveness by attaining the required displacement ductility and load carrying capacity and would be an excellent candidate for post-earthquake retrofit of damaged existing RC structures designed according to different design evolutions.

Keywords: beam-column sub-assemblage, steel bracket and haunch hybrid retrofit, energy dissipation, ductility, damage index, load-displacement hysteresis, strength degradation, post-earthquake retrofit

1. Introduction

The concept of ductility detailing for seismic resistance design of reinforced concrete structures was codified in 1980s but there were plenty of structures which were built before that and designed only for gravity load. In addition to the above, there were lot of existing reinforced concrete (RC) structures with different forms of seismic deficiencies due to lack of the then prevailed knowledge, such as deficient joints, lack of confinement in the disturbed region (D-region) comprising of joint panel and area of column and beam segments adjacent to joint panel, location of lap splicing at critical location and non-availability of sufficient anti-buckling steel to prevent buckling of main reinforcement bars. It is obvious that these structures would underperform in the event of an earthquake. This necessitated formulation of viable repair and retrofit strategies for earthquake damaged deficient existing RC structures. Thus, the retrofitting of damaged or strengthening of undamaged deficient beam-column sub-assemblages is an active area of research and developing a viable retrofit strategy still remains a challenge.

In broader sense, the seismic retrofit of RC structures was carried out using jacketing, FRP strengthening, external strengthening using steel elements and haunch retrofit, external prestressing etc. Jacketing and FRP strengthening are the most commonly used methods of retrofitting and ample research was carried out to evaluate the performance of damaged reinforced concrete structures/structural components retrofitted using these methods. These retrofit interventions were carried out at the structure level on the frames or buildings (Stoppenhagen *et al.* 1995, Bracci *et al.* 1995, Balsamo *et al.* 2005, Corte *et al.* 2006), Kakaletsis *et al.* (2011)) with the view of shifting the soft storey failure to beam sway mechanism or achieve performance level same as that of undamaged or higher. Furthermore, lot of research was reported at sub-assemblage level on either undamaged deficient ones to achieve higher performance levels (Antonopoulos and Triantafillou 2003, Prota *et al.* 2003, Mukherjee and Joshi 2005, Shannag and Alhassan 2005, Tsonos 2008, Kalogeropoulos *et al.* 2016) or damaged and repaired ones to achieve the original performance as that of

*Corresponding author, Ph.D. Student
E-mail: kanchana@serc.res.in
[a] Ph.D.

http://www.techno-press.com/journals/sem&subpage=7
ISSN: 1225-4568 (Print), 1598-6217 (Online)

the undamaged member or higher (Shannag *et al.* 2002, Karayannis and Sirkelis 2008, Tsonos 2008, Garcia *et al.* 2014a, Tsonos 2014, Yurdakul and Avsar 2015, Kalogeropoulos *et al.* 2016). Even though the jacketing and FRP strengthening are successful in achieving the desired performance level, jacketing is highly laborious and needs skillful detailing. On the other hand, FRP strengthening demands suitable anchoring, especially when it comes to strengthening of joints.

More recently, external strengthening of RC structures is gaining popularity due to its ease of application without disturbing the existing structural system. External strengthening of RC structures was accomplished by addition of steel elements to beams and columns using steel angles, steel props and curbs, steel cages, post-tensioned metal straps, buckling-restrained braces, joint enlargement using prestressed steel angles and stiffened steel plates, prestressed steel strips (Garcia *et al.* 2014b, Campione *et al.* 2015, Mahrenholtz *et al.* 2015, Yurdakul and Avsar 2016, Kheyroddin *et al*. 2016, Torabi and Maheri 2017, Adibi *et al.* 2017, Shafaei *et al.* 2017, Kanchanadevi *et al.* 2018, Yang *et al.* 2018). Further, external strengthening was also accomplished by planar joint expansion, SIFCON blocks, steel haunch, wing walls, etc. (Pampanin *et al*. 2006, Chaimahawan and Pimanmas 2009, Misir and Kahraman 2013, Li and Sanada 2017, Kanchanadevi *et al.* 2018). Yurdakul *et al*. (2018) carried out local retrofitting of non-seismically deficient beam-column joint by post-tensioned SMA bars to minimize the damage in the joint panel. It was concluded that SMA bars should be post-tensioned to their yield capacity to derive full benefit from super-elastic property to minimize residual deformation. Duran *et al*. (2019) upgraded the substandard RC frame using shape memory alloy(SMA) bars. The study highlighted that super-elastic property of SMA could be utilised for recovering residual deformations of the moment resisting frame after passage of seismic event. If the SMA bars are in place before the seismic event, the residual deformations can be reduced. It may be noted that SMA is expensive and is not easily available. Most of the external strengthening schemes are aimed at strengthening of the critical components to achieve the desired strength hierarchy. Whereas the haunch retrofit achieves strength hierarchy by reducing the force demand on critical components. Furthermore, haunch retrofit is non-invasive and could be executed with ease.

Yu *et al.* (2000) conceived the idea of welded haunch for steel moment resisting frames which experienced failure at the welds during Northridge earthquake. Further, it was reported that haunch retrofit succeeded in preventing the weld failure in the rehabilitated steel moment connections. This concept of haunch retrofit was extended to reinforced concrete structures by Pampanin *et al.* (2006). The double haunch retrofit solution (with haunches at top and bottom of floor beam) was employed for seismic strengthening of the existing non-seismically designed RC structures. Further, analytical formulations were developed for the design of double haunch retrofit solution. They found that the retrofit succeeded in preventing the failure of joint and succeeded in forming plastic hinges in the beam. In order to make the double haunch scheme more practical to implement, Genesio (2012) connected haunches to the adjacent beam and column segments by means of post-installed chemical anchors. This study confirms that for the optimal retrofit solution, hinges would form in beam and the joint damage could be prevented. Sharma *et al.* (2014) extended the double haunch scheme connection using post-installed chemical anchors for building frame with olden detailing practice and tested it on the shake table. The study concluded that retrofit solution was successful in improving the seismic performance of non-seismically designed RC framed structures. Wang *et al.* (2018) studied the effect of buckling restrained haunches in improving the seismic performance of interior and exterior joints. This study was aimed at relocating the plastic hinges and also to improve the energy dissipation of the system. It was reported that the scheme was successful in achieving the desired performance level. Zabihi *et al.* (2018) carried out parametric study on the performance of beam-column sub-assemblage retrofitted with single and double haunch retrofit and compared with that of non-retrofitted beam-column sub-assemblage. Kanchanadevi and Ramanjaneyulu (2019) evaluated the comparative seismic performance of gravity load designed beam-column sub-assemblages retrofitted using single haunch and single steel bracket and haunch hybrid retrofit at soffit of beam. This study established the superiority of single steel bracket and haunch hybrid retrofit scheme over single haunch retrofit scheme for GLD beam-column sub-assemblages in terms of enhanced load carrying capacity, energy dissipation and sustaining larger drifts.

The reported studies, documented the promising performance of double haunch retrofit solution in achieving the desired performance level at both sub-assemblage and structure levels. Further, it could be noted that the double haunch solution was implemented only for strengthening of the undamaged components and studies were not reported on its usage as retrofit solution for the damaged beam-column sub-assemblages. Furthermore, it was reported that single steel bracket and haunch hybrid retrofit exhibited superior performance over haunch alone retrofit. With that view, in the present study, double steel bracket and haunch hybrid retrofit with one hybrid haunch fixed at the soffit of the beam and the other hybrid haunch fixed to the top face of the beam is used to retrofit the damaged deficient beam-column sub-assemblages of different design evolutions. The study considers three levels of design for the exterior beam-column sub-assemblages representing RC structures of different design evolutions. The beam-column sub-assemblages designed for different design evolutions are tested till failure under reverse cyclic loading. The damaged beam-column sub-assemblages are repaired and then retrofitted using the novel and innovative steel bracket and haunch hybrid retrofit solution developed in the study. The retrofitted specimens are tested again under reverse cyclic loading. The seismic performance of the repaired and retrofitted specimens are compared with undamaged control specimens to demonstrate the efficacy and effectiveness of the proposed retrofit solution for earthquake damaged beam-column sub-assemblages.

2. Details of the beam-column sub-assemblage specimens considered for study

A three storied RC framed residential building as shown in Fig.1(a) is taken up for study. An exterior beam-column

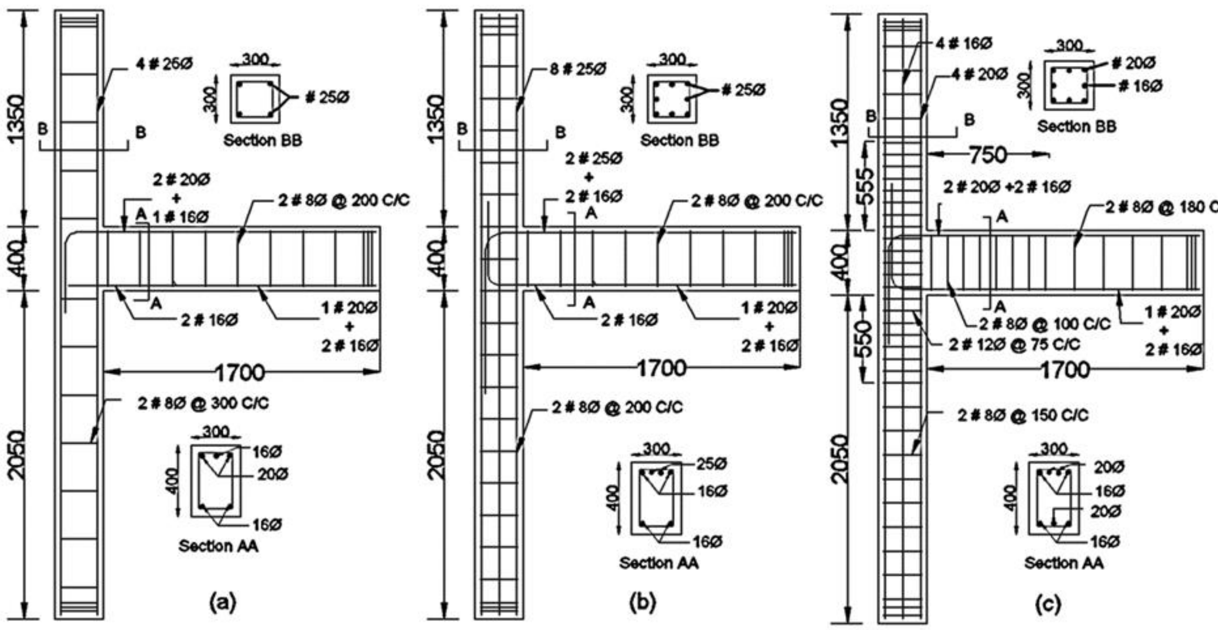

Fig. 1(b) Reinforcement details of (a) SP1 (b) SP2 (c) SP3 beam-column sub-assemblages

sub-assemblage highlighted in Fig.1(a) is chosen for experimental investigations. Exterior beam-column sub-assemblage specimen is designed as per Indian Standards of practice (IS: 456(2000), IS: 1893(2002), IS: 13920(1993)) to represent the existing olden RC structures of Indian sub-continent. Three evolutions of design, namely i) Gravity load designed (SP1: GLD) with straight bar anchorage for reinforcements at beam bottom ii) Seismic load designed but without ductility detailing (SP2: Non-ductile) iii) Seismic load designed with ductility detailing (SP3: Ductile) are considered for the design of specimens. The beam-column sub-assemblages chosen for present study are designed according to olden Indian standard which does not specify explicit provisions for design of joint for ductile specimen. The capacity of joint limited by the concrete struts was not specified in Indian standards which may govern the dimensioning of the joint. Further, in Indian code IS13920(1993), there was no restriction on member sizes namely depth of beam and column, and also member sizes are not the function of diameter of the beam bar to be used. Further, the provisions related to development length of beam bars into joint differ from other international standards like ACI 318 (2011), NZ 3101 (2006), EC 8 (2004). The ductile and non-ductile specimens do not conform to modern seismic guidelines of proportioning of joint to prevent joint shear failure. Hence, the specimen SP3 possesses deficient joint even though it is detailed for ductility.

The overall dimensions of beam-column sub-assemblage along with the cross sectional details of beam and column segments and reinforcement details are depicted in Fig.1(b). Strain gages are affixed on reinforcement bars of the specimens at the identified critical locations before casting of the specimens. Concrete mixture is designed with cement, sand and coarse aggregates in proportion of 1:1.695:3.013 and water-to-cement ratio of 0.5. This concrete mix is used for casting of the beam-column specimens. After casting, the specimens are wet cured for 28 days. The material properties of concrete cylinders cast along with the specimens are evaluated at the time of testing and are given in Table 1. The material properties of steel reinforcement bars used are shown in Table 2. The cross section analysis of the beams and columns are carried out using the standard procedure outlined in Indian code of practice IS 456(2000). The reinforcement details and ultimate design moment capacities evaluated for the beams of different specimens are presented in Table 1. The reinforcement details of columns of different specimens are also presented in Table 1. The ultimate moment versus axial load capacity interaction curves for the columns of different specimens (SP1, SP2 and SP3) are obtained and are presented in Fig. 2.

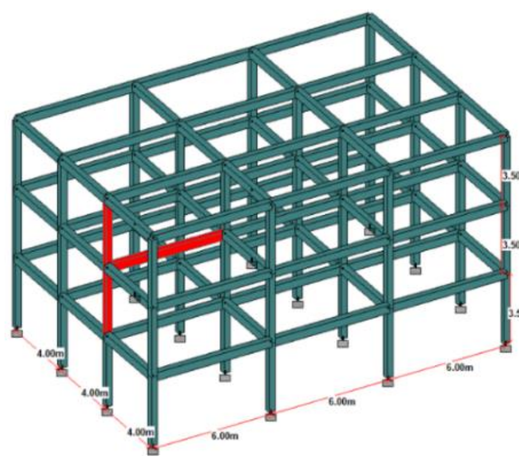

Fig. 1(a) Geometrical details of building and beam-column sub-assemblage chosen for the study

Table 1 Details of specimens chosen for investigations

Specimen ID	Percentage main reinforcement (%)	Shear reinforcement	Ultimate moment capacity (kNm)	Cube compressive strength (N/mm^2)	Average split tensile strength (N/mm^2)
SP1	Beam Top =0.69 Beam bottom=0.33 Column =2.18	Beam -2#8ϕ@200mm c/c Column-2#8ϕ@300mm c/c Joint- Nil	Beam Top= 117 Beam bottom=18*	41.34	3.74
SP2	Beam Top=1.15 Beam bottom=0.33 Column=4.36	Beam -2#8ϕ@200mm c/c Column-2#8ϕ@200mm c/c Joint- 2#8ϕ@200mm c/c	Beam Top=174 Beam bottom=60	39.73	4.15
SP3	Beam Top=0.85 Beam bottom=0.596 Column=2.29	Beam$^+$ -2#8ϕ@100mm c/c Beam$^\$$ -2#8ϕ@180mm c/c Column$^+$-2#12ϕ@75mm c/c Column$^\$$ -2#8ϕ@150mm c/c Joint- 2#12ϕ@75mm c/c	Beam Top= 141 Beam bottom=102	40.91	3.88

+ - In confinement region; $ - Beyond confinement region; * - Moment capacity restricted by actual anchorage length of bottom reinforcement

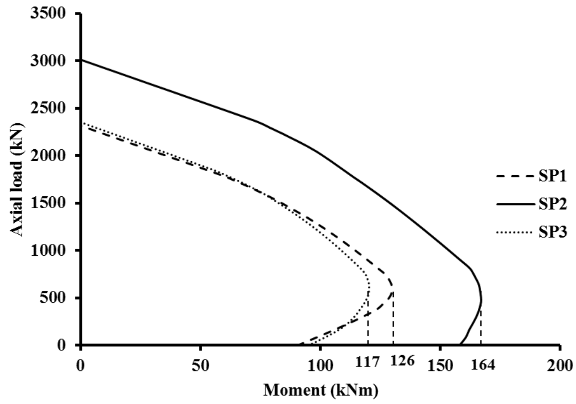

Fig. 2 Ultimate moment versus axial load capacity curves for columns of different specimens

Table 2 Material properties of steel reinforcement bars

Diameter of reinforcement bar (mm)	Average yield strength of steel (N/mm2)	Average ultimate strength of steel (N/mm2)
8	527	641
16	520	647
20	545	621
25	535	643

3. Experimental investigations on undamaged control beam-column sub-assemblages

LVDTs (linear variable displacement transducers) are mounted on the undamaged control beam-column sub-assemblage specimens (SP1, SP2, SP3) to measure deflections. The test setup for applying reverse cyclic loading is arranged horizontally on the test floor as shown in Fig.3. The column axial load is applied by hydraulic jack at one end of column and other end of the column is against the reaction block. An axial load of 300kN is applied to the column which is arrived from analysis of a three storied building shown in Fig.1(a). The reverse cyclic loading is applied by means of servo-controlled hydraulic actuator at beam tip in displacement control mode according to the loading history shown in Fig.4. Reverse cyclic displacements are expressed in terms of drift ratio (%) and is defined according to Eq. (1).

$$\text{Drift ratio}(\%) = \frac{\Delta l}{l_b} \times 100 \qquad (1)$$

Where, Δl is the applied displacement at the beam tip and l_b is the length of the beam from column face to the point of application of the displacement.

In present study, maximum displacements (Δl) applied are: ± 6.25mm, ±12.5mm, ±25mm, ±37.5mm, ±50mm, ±62.5mm, ±75mm, ±87.5mm, ±100mm, ±112.5mm and ±120mm. First two drift increments ± 6.25mm, ±12.5mm are elastic cycles. Yielding occurred at displacement of 25mm. The further drift increments except final drift increment are arrived by constantly increasing displacement with ±12.5mm from previous step and thereby resulting in more inelastic excursions. Due to the restriction of the stroke length of the actuator, the final drift increment is kept as ±7.5mm. For each drift level, three complete cycles are applied with equal magnitude in both positive and negative cycles of loading. The positive drift cycle produces tension at beam bottom and negative drift cycle produces tension at beam top. The data pertaining to load-displacement hysteresis of all the three control specimens (SP1, SP2 and SP3) are acquired and processed. The summary of observations made on the results of experimental investigations carried out on the three types of control specimens are presented in Table 3.

From Table 3, it is very clear that location and the level of damage undergone are different for each type of specimen, even though in all the specimens test was stopped when the load in third cycle of the particular drift ratio is dropped to around 40% of peak load. It is observed that in the GLD specimen SP1, major portion of the beam-column sub-assemblage remains undamaged except a crack at joint. The width of diagonal joint shear crack in SP1 is found to be smaller than that in the specimens SP2 and SP3. This is because of the fact that the specimen SP1 has undergone only 15 cycles of loading before the test is stopped. In the case of specimen SP2, the major portion of beam remains undamaged except for few thin flexural cracks, but the joint and disturbed regions of the column are damaged drastically at final stage of loading. The specimen SP3 has undergone severe damage in the joint region and cover concrete is spalled-off completely during the final stage of loading. Further, the disturbed regions of beam as well as column segments are also damaged in the specimen SP3, as the specimen has undergone more number of loading reversals when compared with the other two specimens tested.

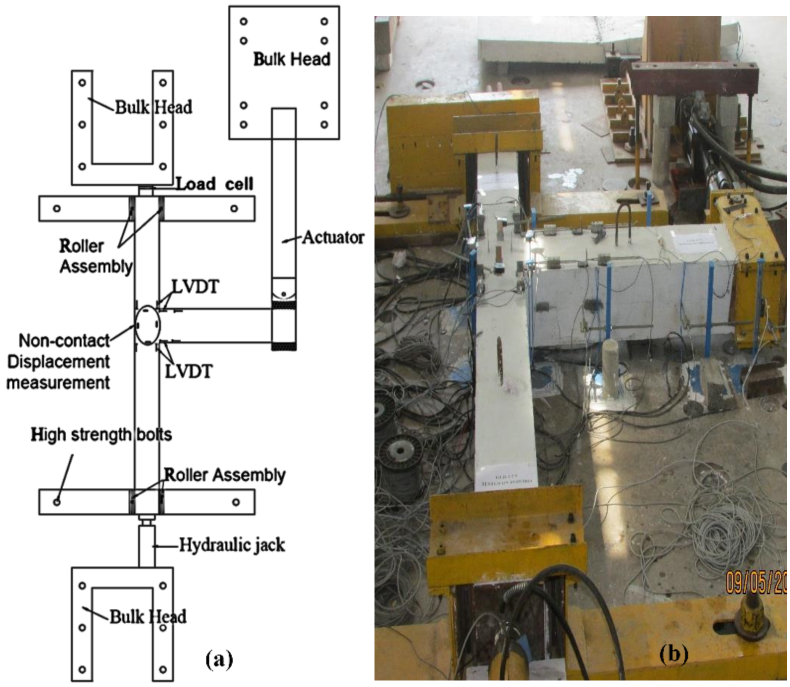

Fig. 3. (a) Schematic and (b) Actual test-setup and instrumentation for experimental investigations

Table 3 Summary of observations for all the three types of undamaged control specimens

Description	SP1 (GLD)		SP2 (Non-Ductile)		SP3 (Ductile)	
Peak Load in +ve and –ve cycles	+39 kN	-85kN	+58kN	-112 kN	+94 kN	-123 kN
Final drift ratio	2.94%		5.88%		7.05%	
No. of cycles till final drift ratio	15		27		33	
Load at final +ve and –ve drift cycle	+15 kN	-54 kN	+18 kN	-44 kN	+52 kN	-52 kN
Damage undergone after final drift ratio	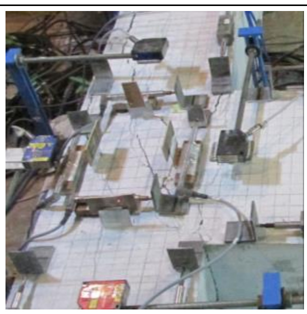		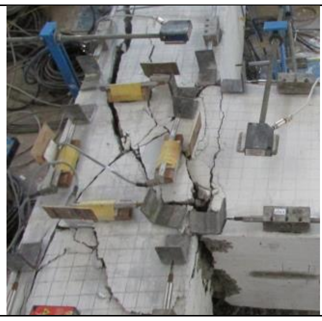			

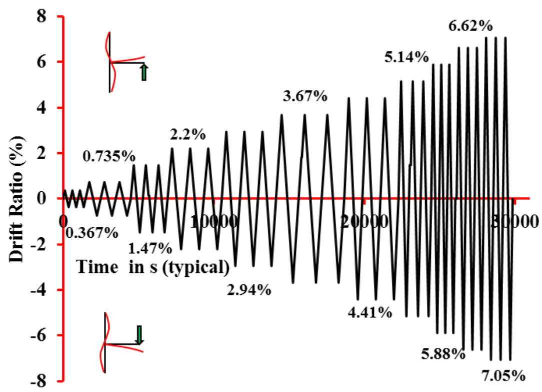

Fig. 4. Typical reverse cyclic loading history

4. Repair of beam-column sub-assemblages damaged under reverse cyclic loading

After completion of testing of all the three control beam-column sub-assemblages (SP1, SP2 and SP3) under quasi-static reverse cyclic loading, the damaged specimens are repaired as detailed below. The step-by-step repair procedure is depicted in Fig.5. The cover concrete in the damaged portion of joint, beam and column regions is removed carefully using chisel and hammer (Fig.5 (a)). Care is taken in such a way that the chiselling does not cause any further damage to the core concrete. Further, in the regions of severe cracking, concrete cutting machine is used to cut the slots up to the level of cover concrete and the damaged concrete is removed (Fig.5(b)). After removing the damaged parts of concrete, the specimen is cleaned with wire brush to remove laitances. Then the specimen is cleaned with water jet and allowed to dry. In order to close/fill the cracks in the core concrete, epoxy grouting is carried out. Prior to the grouting operation, the required number of grouting ports are fixed. The maximum spacing of 200mm is maintained between grouting points. Holes are drilled into the core concrete and the steel injection packers are placed inside the holes and the nipples are tightened by using the spanner (Fig. 5(c)). The gap between the steel injection packers and surrounding concrete is sealed by using Lokfix (two-component polyester resin anchoring grout) (Fig. 5(d)). After anchoring the steel injection packers, surface cracks are sealed with Renderoc leak plug, so that the grout will not escape through the surface cracks. The setting time of the leak plug is approximately 1-2 minutes at 30degree centigrade ambient temperature. After suitable surface preparation, the cracks in the core concrete are sealed by grouting (Fig. 5(e)) using Conbextra EP 10, an epoxy based low viscous pressure grout using grouting machine. The grout has a pot life of 50 minutes and the entire grouting operation is carried out before the pot life of the grout.

(a) Removal of damaged cover concrete

(b) Removal of cracked cover concrete

(c) Installation of steel injection packers

(d) Sealing of injection packers

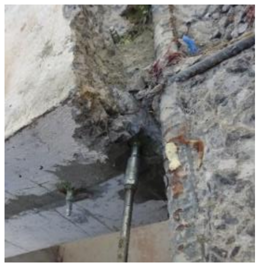

(e) Epoxy grouting of the core concrete

(f) Application of bond coat on existing concrete surface

(g) Re-laying of concrete using non-shrink repair mortar

Fig.5 Step-by-step procedure for repair of damaged beam-column sub-assemblages

After completion of epoxy grouting of the core concrete, the cover concrete is laid by using cementitious precision mortar Conbextra GP2. Conbextra GP2 is a blend of Portland cement, graded fillers and chemical additive in powdered form. Conbextra GP2 is mixed with 8mm downgraded aggregates and water in the ratio of 1:0.5: 0.18 (GP2:8mm aggregates: water). This would yield compressive strength of 60 MPa and flexural strength of 9 MPa (as per Fosroc technical data sheet). At first, an epoxy based bond coat is applied on the old concrete surface (Fig. 5(f)) so as to ensure proper adhesion between the old concrete surface and new cementitious mortar to be laid. The non-shrink repair mortar is laid into the wooden shutters arranged around the joint region and re-laying of beam-column sub-assemblage is carried out (Fig. 5(g)). The re-laid region of the beam-column sub-assemblage is wet cured for 7 days.

5. Steel bracket and haunch hybrid scheme for retrofitting of specimens

5.1 Force flow mechanism of sub-assemblage with double haunch retrofit

The introduction of double haunch near the joint region of beam-column sub-assemblage reduces the bending moment and shear force at joint as shown in Fig.6. The reduction of beam bending moment in turn reduces the shear demand on the joint. The vertical component of haunch force is expressed in terms of non-dimensional parameter β_1, which is defined as the ratio of vertical component of haunch force to beam tip loading.

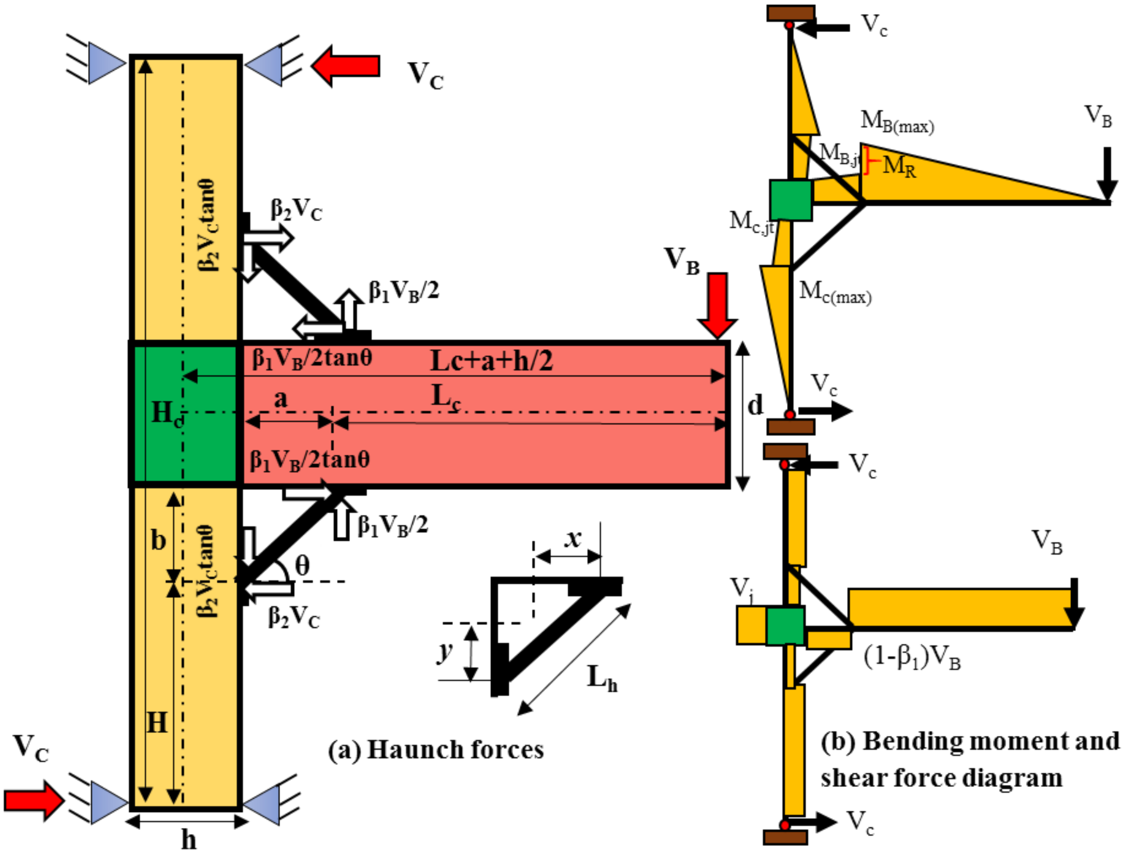

Fig. 6 Force flow, bending moment and shear force in the sub-assemblage after introduction of double haunch

The reduced beam moment ($M_{B,jt}$) at the face of the joint due to the introduction of haunch is given by,

$$M_{B,jt} = V_B(L_c + a) - \beta_1 V_B a - \frac{\beta_1 V_B d}{2\tan\theta} \quad (2)$$

The reduced column moment (Mc, jt) at the face of the joint due to the introduction of haunch is given by,

$$M_{c,jt} = V_C(H + b) - \beta_2 V_C b - 0.5\beta_2 V_C h \tan\theta \quad (3)$$

where V_B and V_C are beam tip loading and column shear respectively. Lc is length of beam between point of contra flexure and haunch-beam connection. d and h are depth of beam and column respectively. θ is orientation angle of haunch. a and b are distances between joint face and haunch connection points at beam and column respectively as shown in Fig.6(a). The haunch force factor for double haunch retrofit under lateral load alone case with integral connection was presented by Pampanin *et al.* (2006). Further, the analytical formulations for evaluation of haunch force factor for single haunch retrofit with integral and post-installed anchor connections are presented by Kanchanadevi and Ramanjaneyulu (2018) for both lateral load alone and combined lateral load and gravity load. In present study, the formulations are presented for combined lateral load and gravity load case for integral connection of double haunch retrofit.

The beam moment at a distance 'x' from the haunch-beam connection is given by,

$$M_x = (L_C + x)V_B - \frac{\beta_1 d V_B}{2\tan\theta} - \beta_1 V_B x \quad (4)$$

The stress induced in the beam at section 'x' from the beam-haunch connection, due to the moment is given by,

$$\sigma_x = \frac{V_B d}{2I_B}(L_C + x - \beta_1 x - 0.5\beta_1 d\cot\theta) \quad (5)$$

The horizontal (Δ_{bh}) and vertical (Δ_{bv}) deformations of beam at the haunch location due to the axial shortening and bending deformation of beam are given by Eq. (6) and (7) respectively,

$$\Delta_{bh} = \int_0^a \frac{\sigma_x dx}{E_c} \quad (6)$$

$$\Delta_{bv} = \int_0^a \frac{M_x \, xdx}{E_c I_B} \quad (7)$$

The moment at a distance 'y' from the haunch-column connection is given by,

$$M_y = (H - 0.5\beta_2 h\tan\theta)V_C + (1 - \beta_2)V_C y \quad (8)$$

The stresses developed at the section 'y' from the column-haunch connection is given by,

$$\sigma_y = \frac{V_C h}{2I_C}(H + y - \beta_2 y - 0.5\beta_2 h\tan\theta) - \frac{\beta_2 V_C \tan\theta}{A_C} \quad (9)$$

Similarly, deformation of column due to axial shortening and bending deformation are evaluated using Eq. (10) and (11) at haunch column connections.

$$\Delta_{ch} = \int_0^b \frac{\sigma_y dy}{E_c} \quad (10)$$

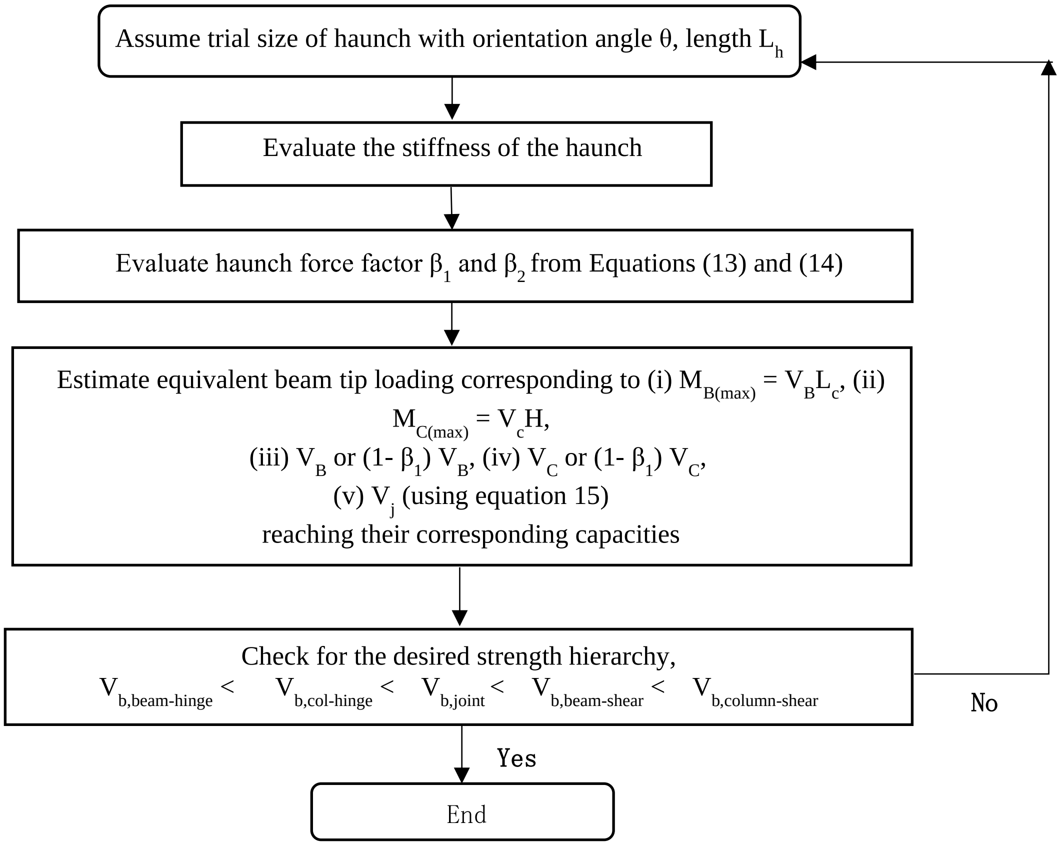

Fig.7 Step-by-step procedure for design of haunch retrofit

$$\Delta_{cv}= \int_0^b \frac{M_y y dy}{E_c I_C} \tag{11}$$

The expression for haunch force factor β_1 could be established by enforcing displacement compatibility between beam-column sub-assemblage and haunch as given by,

$$(\Delta_{bh}\cos\theta + \Delta_{bV}\sin\theta) - (\Delta_{ch}\sin\theta + \Delta_{cv}\cos\theta) = \frac{\beta_1 V_B L_h}{\sin\theta A_h E_s} \tag{12}$$

The expression for haunch force factor β_1 for double haunch, is obtained as follows.

$$\beta_1 = \frac{b}{a}\left[\frac{6L_c d+3ad+6L_c b+4ab+X+Z}{6bd+3d^2+4b^2+\frac{12I_B E_c}{2aK_h\cos^2\theta}+Y}\right] \tag{13}$$

Where $X = \frac{3Hb^2(2L_c+2a+h)I_B}{aH_C I_C} + \frac{2b^3(2L_c+2a+h)I_B}{aH_C I_C}$ (13a)

$$Z = \frac{3Hhb^2(2L_c+2a+h)I_B}{a^2 H_C I_C} + \frac{3hb^3(2L_c+2a+h)I_B}{2a^2 H_C I_C} \tag{13b}$$

$$Y = \frac{3h^2 b^3 I_B}{2I_C a^3} + \frac{6b^3 I_B}{A_C a^3} + \frac{3b^3 h I_B}{I_C a^2} + \frac{2b^3 I_B}{I_C a} \qquad 13(c)$$

Based on the equilibrium of forces, the relation between β_1 and β_2 could be established and given by Eq. (14).

$$\beta_2 = \frac{\beta_1 H_C}{(2L_c+2a+h)\tan\theta} \tag{14}$$

where, A_c= area of cross section of column; A_b= area of cross section of beam; E_c= Young's Modulus of concrete; I_B= effective moment of inertia of beam; I_C= effective moment of inertia of Column; $K_h=A_hE_s/L_h$ is the stiffness of the haunch. A_h= area of cross section of haunch; E_s= Young's Modulus of steel; L_h= Length of haunch.

The reduced joint shear (Vj) due to the introduction of haunch is given by,

$$V_j = \frac{M_{B,jt}}{jd} - (V_c - \beta_2 V_C) \tag{15}$$

Where jd- is lever arm distance of beam.

Step-by-step procedure for the design of haunch retrofit is presented in Fig.7. By varying the cross section, length and orientation of the angle of the haunch, the value of haunch force factor β_1 could be varied. In this procedure, if the haunch yields, the horizontal and vertical components of the haunch force are restricted to the yield strength of the haunch. By appropriate selection of haunch geometry, the desired strength hierarchy (i.e. flexural hinging of beam should occur first before the other modes of failure) of sub-assemblage could be arrived.

5.2 Development and design of steel bracket and haunch hybrid retrofit

The primary function of haunch is to provide the alternate force path and to reduce the demand on the joint. The portion of beam near the intersection of beam and column of deficient specimens would incur severe damage under reverse cyclic loading. It is observed that by providing bracket, cracking at the joint can be prevented

(Kanchanadevi *et al.* (2018)). Since the retrofit scheme is being proposed for damaged specimens, it is essential to strengthen this portion. Hence, steel brackets are provided to strengthen the portion of beam near the intersection of beam and column. The steel bracket and haunch hybrid retrofit scheme (Fig.8(a)) combines the merits of both steel bracket and steel haunch. Steel bracket and haunch are connected by means of two steel square rods as shown in Fig. 8(a) in order to prevent the buckling of the haunch.

The haunch retrofit for the beam-column sub-assemblage specimens is designed using the procedure outlined in Fig.7. For GLD specimen, in order to prevent anchorage failure of beam bottom bars (16mm bars require development length of 560mm and length of bars projected into the column is 210mm), the haunches are connected at 400mm from the inner face of the column. For specimens SP2 and SP3, the purpose of the retrofit is to prevent the joint shear failure and as the specimens are seismic load designed, improvement in load carrying capacity is not needed and hence, the haunch can be connected to the beam at distance as close as possible from the joint face, but should prevent joint shear failure. After several trials (as per procedure specified in Fig.7 for designing of the haunch retrofit), a distance of 300mm between haunch connection and the joint face is arrived for seismic load designed specimens SP2 and SP3. A 25mm square haunch with 45 degree orientation angle with the horizontal is adopted for all the specimens. Thus, the length of haunch is 565mm for retrofit of GLD (SP1) and it is 425mm for seismic load designed specimens (SP2 and SP3).

The haunches are designed to yield at the yielding of beam top reinforcement. The geometrical and connection details of hybrid haunch retrofit are given in Figs.8 (a) and (b) respectively. The ends of haunch are also stiffened by two triangular plates at each end as shown in Figs. 8(a) and (b). The gravity load designed (SP1), non-ductile (SP2) and ductile (SP3) specimens which were damaged during reverse cyclic loading are repaired and then retrofitted with double steel bracket and haunch hybrid retrofit systems (one each at top and bottom faces of beam as shown in Fig.8(b)) and are designated as SP1-R1, SP2-R1 and SP3-R1 respectively. For the sub-assemblages shown in Fig.1(b), the effective moment of inertias of the beams are evaluated from the curvature analysis of the section and used for evaluation of haunch force factors β_1 and β_2 for retrofitted specimens (SP1-R1, SP2-R1, SP3-R1). The haunch force factors are presented in Table 4.

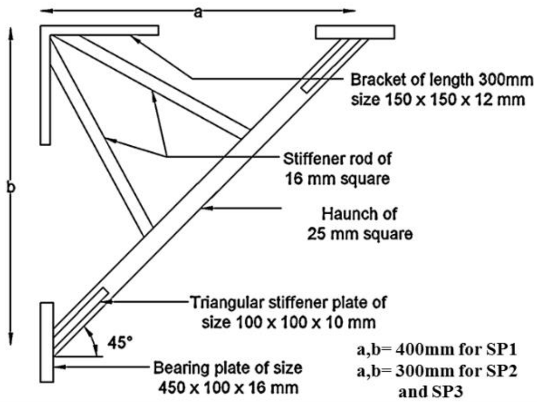

Fig. 8(a) Geometrical details of steel bracket and haunch hybrid retrofit

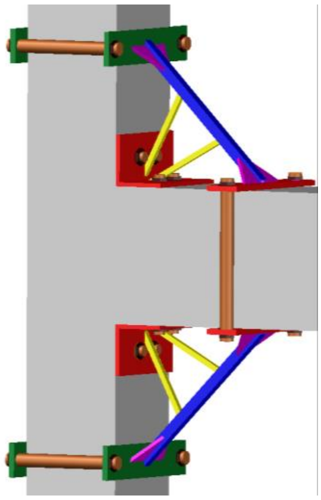

Fig. 8(b) 3D view of steel bracket and haunch hybrid retrofit

Table 4 Haunch force factors for the retrofitted specimens

Specimen	β_1	β_2
SP1-R1	1.96	2.02
SP2-R1	1.77	1.82
SP3-R1	1.88	1.94

5.3 Strength hierarchy of control and retrofitted specimens

The strength hierarchy of the control (SP1, SP2 and SP3) and double haunch retrofitted (SP1-R1, SP2-R1 and SP3-R1) beam-column sub-assemblages are established in terms of equivalent beam tip loading (V_B). Five modes of failure namely, beam shear failure (B_s), beam flexure failure (B_f), column flexure failure (C_f), column shear failure (C_s) and joint shear failure (J_s) are considered for arriving at strength hierarchy of control and retrofitted specimens. The flexural and shear capacities of the beams and columns are evaluated based on IS 456(2000). The shear strength of unreinforced joint of specimen SP1 is evaluated as capacity corresponding to principal tensile stress reaching a value of $0.42\sqrt{f_c}$, where f_c is compressive strength of concrete. For other two specimens SP2 and SP3, the joint shear strength is evaluated based on softened strut and tie model proposed by Hwang and Lee (1999). The strength hierarchy evaluated for beam-column sub-assemblages before and after introduction of hybrid haunch retrofit is shown in Fig.9(a) and (b) respectively. It could be observed from Fig.9(a) that all the three control specimens SP1, SP2 and SP3 showed joint shear mode of failure prior to the introduction of retrofit. After the introduction of the haunch retrofit, the mode of failure of the repaired and retrofitted specimens (SP1-R1, SP2-R1 and SP3-R1) changed from joint shear failure to beam flexural failure as can be witnessed from Fig. 9(b).

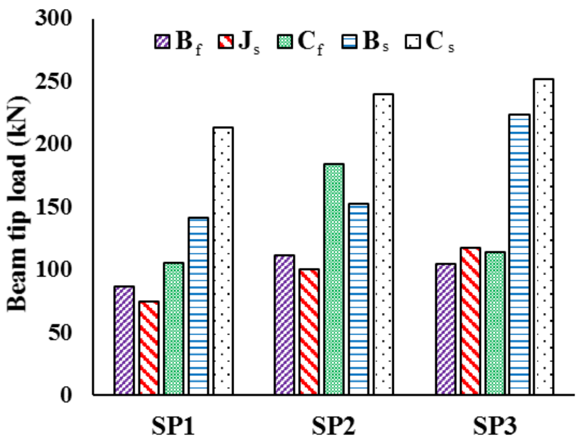

(a) Before retrofit

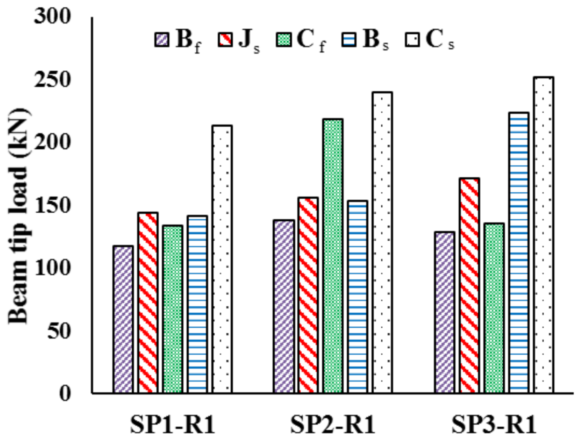

(b) After retrofit

Fig.9 Strength hierarchy of specimens before and after introduction of double haunch retrofit

6. Comparative seismic performance of hybrid haunch retrofitted and control beam-column sub-assemblages

The retrofitted beam-column sub-assemblages namely SP1-R1, SP2-R1, SP3-R1 are tested under reverse cyclic loading using the loading protocol shown in Fig.4. The seismic performance of the repaired and retrofitted specimen is compared with the corresponding control specimen in terms of load-displacements, strength degradation, displacement ductility, energy dissipation, viscous damping and damage index and the results are discussed in the succeeding section.

6.1 Load displacement behaviour of specimens

The load-displacement hysteresis curves obtained for the undamaged control (SP1) and retrofitted (SP1-R1) GLD specimens are shown in Fig.10. The control specimen SP1 showed poor hysteretic performance as it encounters anchorage failure of beam bottom reinforcement bars during the positive cycle of loading at the displacement cycle of 25mm (+1.47%) marked as A and this could be witnessed by opening up of wide joint crack as shown in Fig.10 as damage at A. During the negative cycle, at 50mm (-2.94%) marked as B, the specimen had undergone joint shear degradation as shown in Fig.10 due to the absence of transverse reinforcement in joint region as in a typical olden construction practice. But the repaired and retrofitted GLD specimen SP1-R1 showed superior hysteretic performance when compared with that of the control GLD specimen SP1 in terms of both load carrying capacity and sustaining larger drift levels. During the positive cycle of loading, the damage progression had happened in the form of widening of flexural crack (which is developed at the location of construction joint between the re-laid and old concrete in the repaired specimen) in the closer vicinity of the joint as shown in Fig.10 as damage at A′. With further drift increments, the flexural cracks at construction joint are widened during the positive cycle, and hence, increase in the load carrying capacity beyond the control specimen is not observed in repaired and retrofitted specimen. However, the provision of double hybrid haunch retrofit successfully prevented the brittle anchorage failure of beam bottom reinforcement bars and the specimen SP1-R1 sustained very large drift ratio of about +5.88% (100mm) compared with 2.94% (50mm) sustained by control specimen SP1. There is huge improvement in the load carrying capacity of the specimen SP1-R1 compared with that of the control specimen SP1 in the negative cycle of loading due to the haunch action. During the negative cycle of loading, the failure mode of the repaired and retrofitted specimen SP1-R1 changed from joint shear failure to beam flexural failure and little damage is witnessed in the joint as shown in Fig.10 as damage at B′.

The load-displacement hysteresis curves obtained for the control (SP2) and repaired and retrofitted (SP2-R1) non-ductile specimens are shown in Fig. 11. In the specimen SP2, the load has increased till the drift ratio of +2.2 % (37.5mm) in both positive and negative cycles of loading and from the drift ratio of +2.94% (50mm) uniform strength degradation is observed as shown in Fig.11 due to joint shear degradation. But the specimen SP2-R1 showed enhanced hysteretic performance when compared with that of the control specimen SP2 by sustaining larger drift ratios without strength degradation. The damage incurred by the control (marked as A and B) and retrofitted specimens (marked as A′ and B′) at the drift ratio of 2.94% (50mm) of the non-ductile specimen are shown in Fig.11. From Fig.11, it could be observed that damage progression in control non-ductile specimen SP2 is predominantly through joint shear degradation which is witnessed by wide diagonal cracking of joint. In the case of specimen SP2-R1, even though the specimen showed joint cracks, the crack width is smaller than that in SP2 and also beam flexural cracking is observed as shown in Fig.11. The specimen SP2-R1 carried larger peak load when compared with that of the specimen SP2 during the positive cycle of loading but during the negative cycle of loading, the specimen SP2-R1 carried slightly lower peak load when compared with that of the specimen SP2. Even though the repaired and retrofitted specimen SP2-R1 carried slightly lower peak load in the negative cycle, it sustained the maximum load till the drift ratio of 5.88% (100mm) in both positive and negative

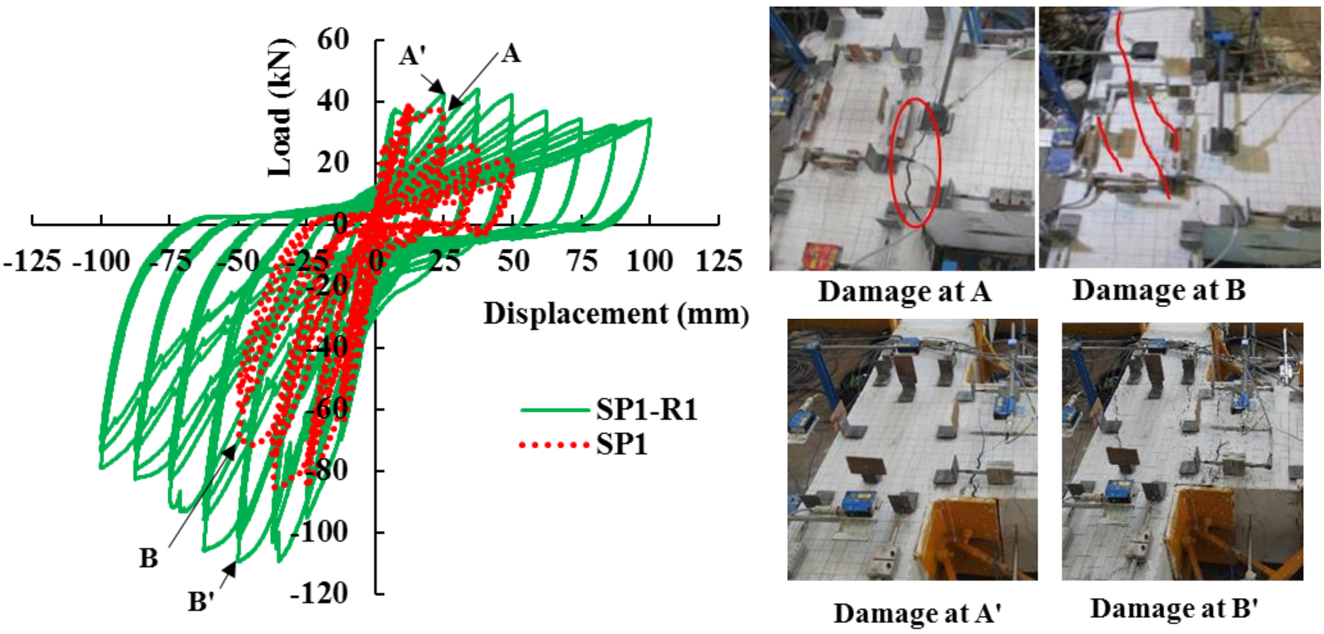

Fig.10. Load displacement hysteresis curves of undamaged control (SP1) and repaired and retrofitted (SP1-R1) beam column sub-assemblages

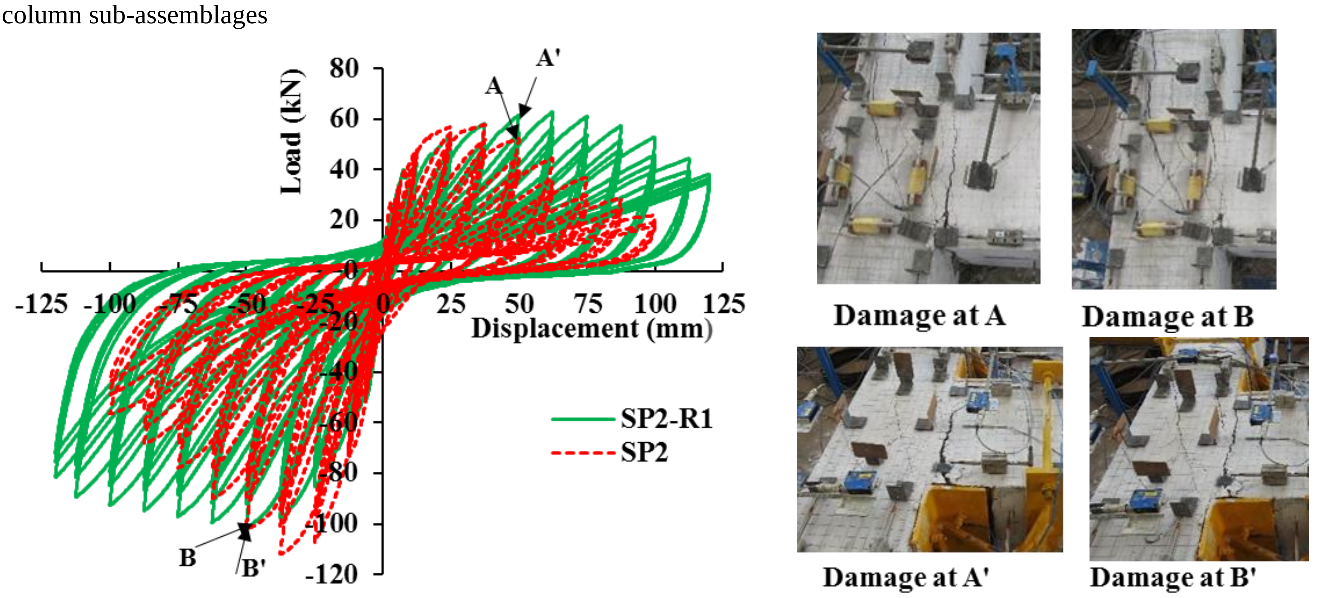

Fig.11. Load-displacement hysteresis curves of undamaged control (SP2) and repaired and retrofitted (SP2-R1) beam-column sub-assemblages

cycles. This is due to the formation of the beam plastic hinge and the major damage progression had happened in the form of flexural cracking of beam even though the joint region has suffered damage. The repaired and retrofitted specimen SP2-R1 could meet the expected ductility performance level displacement of 75mm (4.41%) by sustaining nearly same peak load in both positive and negative cycles of loading without strength degradation.

The load-displacement hystereses obtained for the control (SP3) and repaired and retrofitted (SP3-R1) ductile specimens are shown in Fig. 12. The specimen SP3 sustained maximum load till the displacement level of 87.5mm (+5.14%) and 62.5mm (-3.67%). The damage incurred by the control ductile specimen SP3 at the drift ratio of +5.14% and -3.67% are marked as A and B respectively in Fig.12. From Fig. 12, it may be noted that, the retrofitted specimen SP3-R1 showcased better performance even though joint failure could not be avoided. The damage progression happened in mixed mode i.e. joint cracking and beam flexural cracking in the case of specimen SP3-R1 and finally through joint shear degradation beyond displacement of 112.5mm (+6.61%) and -100mm (-5.88%) in positive and negative cycles of loading respectively. The damage incurred by the repaired and retrofitted specimen at drift ratio of +5.14% and -3.67% (i.e. at the beginning of strength degradation in control specimen SP3) are marked as A′ and B′ respectively as shown in Fig.12. It could be observed that the repaired and retrofitted specimen showed better damage progression when compared with control specimen SP3. The specimen

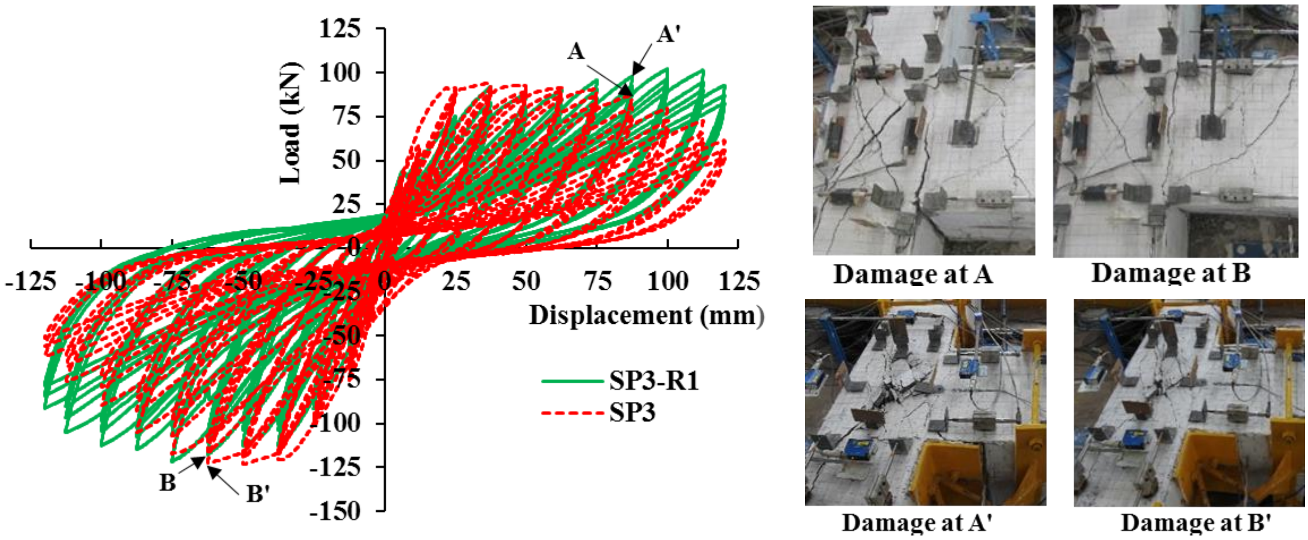

Fig.12. Load displacement hystereses of control (SP3) and repaired and retrofitted (SP3-R1) beam-column sub-assemblages

SP3-R1 carried slightly higher peak load when compared with the specimen SP3 in the positive cycle of loading. In the negative cycle, both specimens carried same peak load. But the peak loads are attained at different drift ratios. During the positive cycle of loading, the specimen SP3-R1 carried peak load at the drift ratio of +5.88% (100mm), whereas the specimen SP3 carried maximum load at the drift ratio of +2.2% (37.5mm). During negative cycle of loading, the specimen SP3 carried maximum load at the drift ratio of -2.94% (50mm) and the retrofitted specimen SP3-R1 carried the maximum load at the drift ratio of -4.41% (75mm). The specimen SP3 exhibited strength degradation behaviour after the drift ratio of +5.14% and -3.67% in the positive and negative cycles of loading respectively. The specimen SP3-R1 sustained the maximum load till the drift ratio of +6.61% (112.5mm) in positive cycle. In the negative cycle, peak load is sustained till the drift ratio of -5.88% (100mm) with less than 15% degradation in the peak load. Even though the joint shear cracks are appeared in SP3-R1 at the drift ratio of -1.47%, the strength degradation had happened after the drift ratio of -5.88% during the negative cycle and this may be due to the reduction of joint shear demand due to the haunch action.

In specimen SP3-R1, joint shear could not be avoided due to following reason. In the case of specimen SP3, the joint was damaged completely at higher drift ratios during the reverse cyclic loading, unlike the other two specimens tested where in the joint damage is relatively less. Furthermore, the repair mortar used for joint repair is cementitious mortar with tensile strength nearly same as that of parent concrete. After initial cracking of joint at the drift ratio of +1.47%, the joint strength depleted due to material softening behaviour of the repair mortar which ultimately resulted in the joint shear failure at larger drift cycles. This could be overcome by using fibre reinforced concrete for repair of damaged joint panel region.

The length of plastic hinge is evaluated based on the analytical expression given by Paulay and Priestley (1992) and presented in Eq. (16).

$$L_p=0.08L+0.022d_bf_y \qquad (16)$$

Where L_p is length of plastic hinge, L is length of beam and d_b is the diameter of reinforcement bar and f_y is yield stress of longitudinal reinforcement. The length of plastic hinge ($L_{P,Ana}$) estimated using Eq.16 is presented in Table 5. The plastic hinge length is also evaluated experimentally as length of extensively damaged zone as suggested by Elmenshawi *et al*. (2012). Accordingly, the length of plastic hinge ($L_{P,Exp}$) is evaluated for all the specimens as length of damaged portion at ultimate deformation (δ_u) and are presented in Table 5. The ultimate deformation (δ_u) is the post-peak deformation corresponding to 15% drop in peak load.

The load-displacement envelopes obtained for the undamaged control and retrofitted specimens are shown in the Fig. 13. The maximum load carried by the control GLD specimen SP1 during the positive and negative cycles of loading are 39kN and 85kN respectively. Whereas the maximum load carried by the repaired and retrofitted GLD specimen SP1-R1 during the positive and negative cycles of loading are 43kN and 109 kN respectively. The maximum load carried by the control non-ductile specimen SP2 are found to be 58kN and 112kN in positive and negative cycles respectively. The maximum load carried by the repaired and retrofitted non-ductile specimen SP2-R1 are found to be 63kN and 102kN in positive and negative cycles respectively. The maximum load carried by the control ductile specimen SP3 are found to be 94kN and 123kN in positive and negative cycles respectively. The maximum load carried by the repaired and retrofitted ductile specimen SP3-R1 is found to be 102kN and 122kN in positive and negative cycles respectively. The load envelopes obtained for the repaired and retrofitted specimens would give insight into the improvement in load carrying capacity and enhancement in capacity to sustain the peak load till larger drift ratios. The encircled portions of the load–displacement curves of beam-column sub-assemblages shown in Fig.13 clearly highlight the superior

Table 5 Length of plastic hinge of control (SP1, SP2, SP3) and retrofitted (SP1-R1, SP2-R1, SP3-R1) specimens

Specimen ID	Beam top				Beam bottom			
	δ_u (mm)	$L_{P,Ana.}$ (mm)	$L_{P,Exp.}$ (mm)	Nature of hinge	δ_u (mm)	$L_{P,Ana.}$ (mm)	$L_{P,Exp.}$ (mm)	Nature of hinge
SP1	49	312	10	No hinge formation	30	300	3-5	No hinge formation
SP1-R1	57	399	10	No hinge formation	55	300	25	No hinge formation
SP2	88	344	300	Mixed mode failure	100	344	275	Mixed mode failure
SP2-R1	75	312	400	Flexural hinge	62	300	150	-
SP3	113	399	275	Flexural hinge	98	300	275	Flexural hinge
SP3-R1	115	344	300	Mixed mode failure	120	344	300	Mixed mode failure

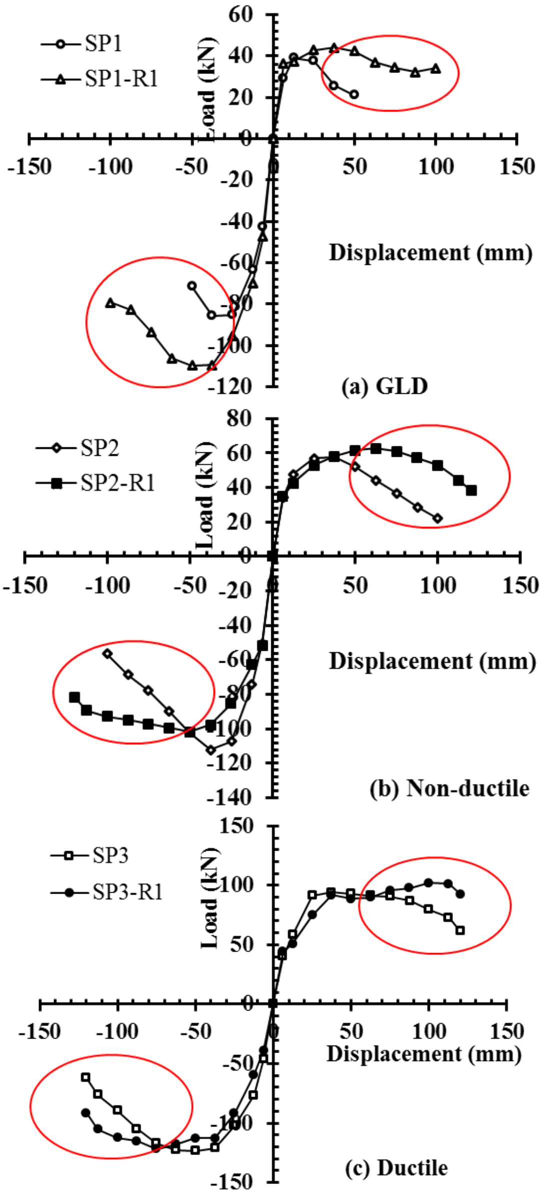

Fig. 13 Load displacement envelopes of control and retrofitted beam-column sub-assemblages

post-peak performance demonstrated by repaired and retrofitted specimens compared with corresponding control specimens.

6.2 Global strength degradation

Degradation in global strength of control and retrofitted specimens, with the increment in drift ratio is shown in Fig.14. Global strength degradation is evaluated as reduction in the strength corresponding to first cycle of each drift ratio with respect to the peak load, after attaining peak load. In the case of control GLD specimen SP1, the beginning of strength degradation took place at the drift ratio of 1.47% during positive cycle. Whereas, in the case of retrofitted GLD specimen SP1-R1, the strength degradation began at the drift ratio of +2.94%. In retrofitted specimen SP2-R1, strength degradation is less than 15% at drift ratio of 5.88% (i.e. maximum drift sustained by control non-ductile specimen SP2) in both positive and negative cycles of loading. Whereas, the control specimen SP2 showed strength degradation of 50% and 62% respectively in positive and negative of cycles of loading at the drift ratio of 5.88%. At 7.05% drift ratio, the control and retrofitted ductile specimens SP3 and SP3-R1 showed strength degradation of 35% and 9.27% respectively in positive cycle. In the negative cycle, SP3 and SP3-R1 showed strength degradation of 50% and 25% respectively at -7.05%. Thus, all the repaired and retrofitted beam-column sub-assemblages exhibited lower strength degradation behaviour when compared with that of the corresponding control beam-column sub-assemblages.

6.3 Displacement ductility

The displacement ductility ratio is defined as the ratio of post-peak displacement corresponding to 85% of the ultimate load to that of the yield displacement (EC8 (2004)). Based on the data acquired during the testing of all the beam-column sub-assemblages, the displacement ductility of the specimens is evaluated using Eq. (17) and are presented in Table 6.

$$\mu = \frac{\Delta_{max}}{\Delta_{yield}} \tag{17}$$

Where, Δ_{max} = Post-peak displacement corresponding to 85% of peak load;
Δ_{yield} = displacement corresponding to yielding of steel.

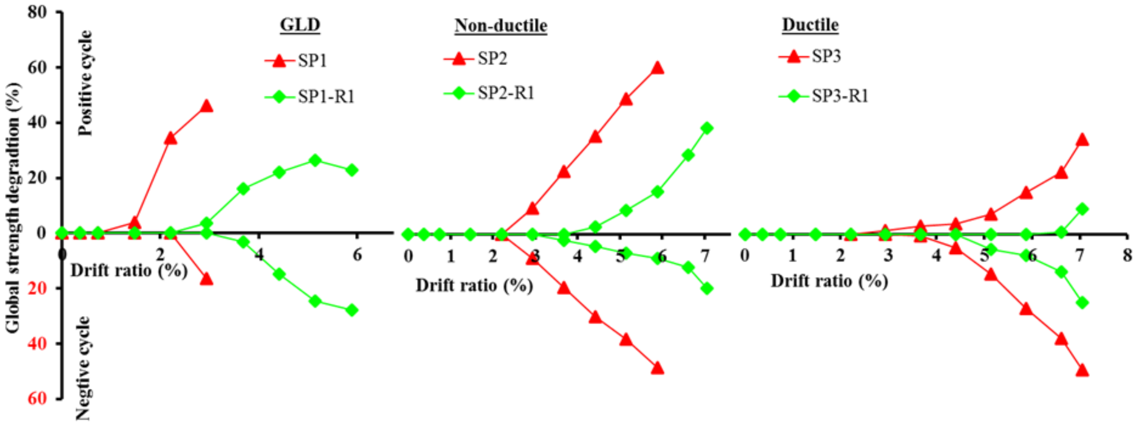

Fig.14. Global strength degradation of control and retrofitted specimens

Table 6 Displacement ductility (μ) of control (SP1, SP2, SP3) and retrofitted (SP1-R1, SP2-R1, SP3-R1) specimens based on experimental study

Specimen ID	Ductility (μ) (in positive cycle)	Ductility (μ) (in negative cycle)	Response reduction factor (R)	Maximum expected Ductility μ_e
SP1	Bars not yielded	2	NA	NA
SP1-R1	*	3	NA	NA
SP2	2	2	3	3
SP2-R1	3	4.5	3	3
SP3	4	3.5	5	5
SP3-R1	5	4.5	5	5

* the construction joint restricted the load carrying capacity and bars have not yielded at that load level

The global yield point is calculated from equivalent bilinear curves of the test specimens based on reduced stiffness equivalent elasto-plastic yield. This yield point is found to be closer to the displacement corresponding to the yielding of beam reinforcement bars. This may be due to the fact that in all the specimens, yielding of reinforcement bars occurred prior to the joint degradation. Hence, the global yield point is characterised by the yielding of steel bars in the cases considered in the study.

IS 1893 (2002) recommends a response reduction factor of 3 and 5 for ordinary moment resisting frames (OMRF) i.e. non-ductile frames and special moment resisting frames (SMRF) i.e. ductile frames. Response reduction factor is the factor by which base shear that would be generated if the structure were to remain elastic during its response to the Design Basis Earthquake (DBE) shaking, shall be reduced to obtain the design lateral force. In present study, the non-ductile and ductile specimens are designed using response reduction factor of 3 and 5 respectively. The response reduction factor is the measure of the perceived seismic performance of the structure under earthquake. As the structure is designed for lesser seismic force, it is expected to have ductility proportional to the response reduction factor. Hence, the beam-column sub-assemblages SP2 and SP3 are expected to have displacement ductility of 3 and 5 respectively in the absence of over strength. This is the limiting case. From Table 6, it may be noted that the retrofitted GLD specimen SP1-R1 had a displacement ductility of three during negative cycle of loading. The control specimen SP2 could reach the displacement ductility of two in both positive and negative cycles of loading. Whereas, the specimen SP2-R1 attained the expected displacement ductility of three in positive cycle and much more than the expected displacement ductility of three in negative cycles. In the case of specimen SP3-R1, the retrofit succeeded in bringing back the load carrying capacity of the repaired and retrofitted specimen to the level of undamaged control ductile specimen SP3. The specimen SP3 could reach displacement ductility of 4 and 3.5 in positive and negative cycles of loading respectively. On the other hand, the specimen SP3-R1 attained displacement ductility of 5 and 4.5 in positive and negative cycles of loading respectively closely meeting the expected displacement ductility of 5. The retrofitted specimens demonstrated the suitability of hybrid haunch retrofit for use in seismic zones.

6.4 Energy dissipation

The cumulative energy dissipated by control and retrofitted specimens are shown in Fig.15. It may be observed from Fig. 15(a) that cumulative energy dissipated by the retrofitted specimen SP1-R1 is far greater than that of the control specimen SP1 for all the drift ratios. The total cumulative energy dissipated by the specimens SP1 and SP1-R1 are 11.65 kNm and 75.9 kNm respectively. The

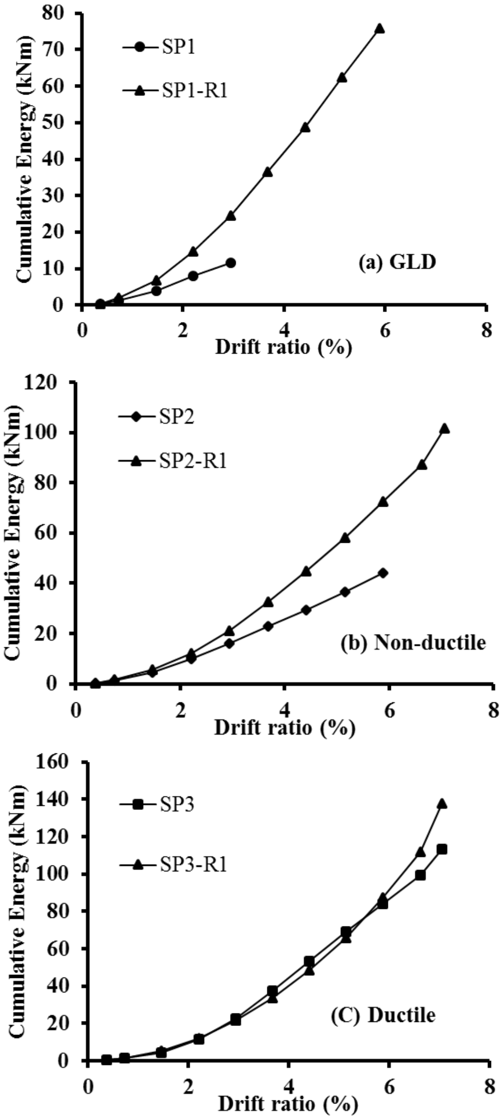

Fig. 15 Cumulative energy dissipated by undamaged control and retrofitted beam-column sub-assemblages

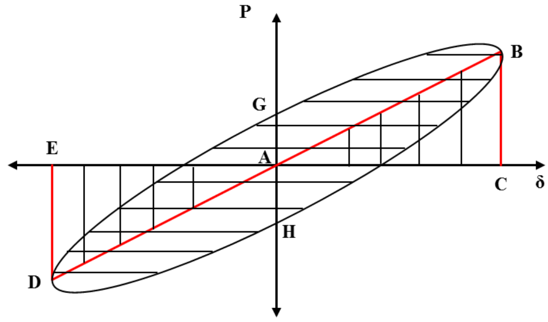

Fig. 16 Model for evaluation of equivalent viscous damping co-efficient

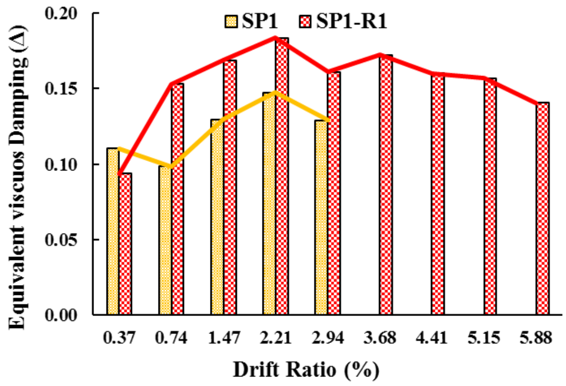

(a) GLD

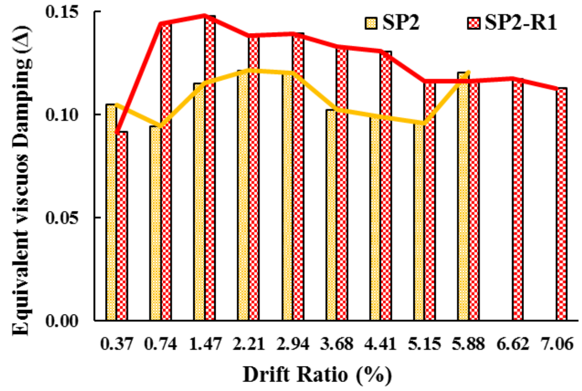

(b) Non-ductile

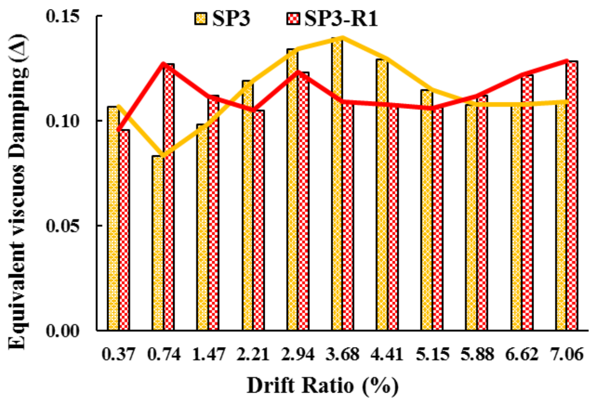

(c) Ductile

Fig. 17 Equivalent viscous damping co-efficient of control and retrofitted beam column sub-assemblages

total cumulative energy dissipated by the repaired and retrofitted GLD specimen SP1-R1 is nearly 6.5 times that of the control specimen SP1. This tremendous improvement in the energy dissipation capacity of the repaired and retrofitted GLD specimen is due to the prevention of anchorage failure of beam bottom reinforcement bars during the positive cycles and delaying the shear damage of the joint in the negative cycles.

From Fig. 15(b), it may be observed that the repaired and retrofitted non-ductile specimen SP2-R1 dissipated nearly the same energy as that of the control specimen SP2 till the drift ratio of 1.47%. Beyond that drift ratio, the energy dissipated by SP2 is lower than that of SP2-R1 in all the subsequent drift ratios. At the final stage of loading of SP2, i.e. at the drift ratio of 5.88%, the cumulative energy dissipated by specimens SP2 and SP2-R1 are 44 kNm and 72.5 kNm respectively. The cumulative energy dissipated by the repaired and retrofitted specimen SP2-R1 till the drift ratio of 5.88% is nearly 1.64 times that of control specimen SP2. Further, the total cumulative energy dissipated by the

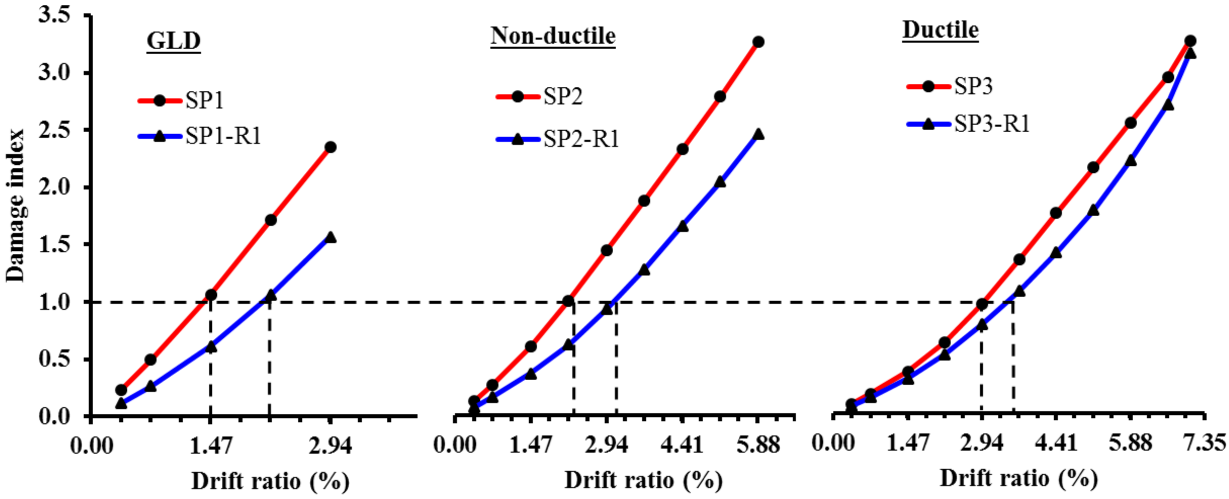

Fig.18 Comparison of damage indices of control and retrofitted specimens

specimen SP2-R1 is 101.79 kNm as against 44 kNm of SP2. Thus, the total cumulative energy dissipated by the repaired and retrofitted specimen SP2-R1 is 2.31 times that of control specimen SP2.

From Fig. 15(c), it may be observed that cumulative energy dissipated by the repaired and retrofitted ductile specimen (SP3-R1) is nearly same as that of the undamaged control specimen SP3 till the drift ratio of 2.94%. For the drift ratios between 2.94% and 5.14%, the energy dissipated by repaired and retrofitted specimen SP3-R1 is little lower than energy dissipated by undamaged control specimen SP3. Beyond the drift ratio of 5.14%, the energy dissipated by the retrofitted specimen SP3-R1 is greater than that of the control specimen SP3 till the drift ratio of 7.05%. The total cumulative energy dissipated by the retrofitted specimen SP3-R1 and the control specimen SP3 are 137.6 kNm and 113.3 kNm respectively. Thus, the total cumulative energy dissipated by the repaired and retrofitted ductile specimen SP3-R1 is 1.21 times that of the control specimen SP3.

6.5 Equivalent viscous damping

The dissipated energy could also be expressed in terms of equivalent viscous damping co-efficient Δ. The equivalent viscous damping co-efficient (Δ) is evaluated based on the model shown in Fig.16 and represented in Eq. (18).

$$\Delta = \frac{1}{2\pi} \frac{Area\ of\ hystersis\ loop\ DGBHD}{Area\ under\ triange\ ABC + Area\ under\ triangle\ ADE} \quad (18)$$

The values of equivalent viscous damping coefficient evaluated for control and retrofitted specimens are presented in Fig.17. From Fig.17(a), it could be observed that there is considerable improvement in damping properties of retrofitted GLD specimen SP1-R1 when compared with the control GLD specimen. Similarly, the retrofitted non-ductile specimen SP2-R1 showed marked improvement in viscous damping co-efficient. The retrofitted specimen SP3-R1 showed higher viscous damping when compared with specimen SP3 till the drift ratio of 1.47% and beyond the drift ratio of 5.14%. But its viscous damping co-efficient is lower than that of undamaged specimen SP3 for the drift ratios between 1.47% and 5.14%. This is due to the difference in the drift level at which the peak loads are attained by control and retrofitted specimens. In control specimen SP3, peak loads are attained at +2.2% and -2.94%. Whereas, in the case of retrofitted specimen SP3-R1, peak loads are attained at +5.88% and -4.41% respectively during positive and negative cycles. From Fig.17, it may be noted that all the repaired and retrofitted specimens showcased enhanced viscous damping.

6.6 Evaluation of damage Index

Park and Ang (1985) model as given in Eq. (19) is used to evaluate damage index (D) of beam-column sub-assemblages tested under reverse cyclic load. This damage model uses the linear combination of ultimate deformation and hysteretic energy for evaluation of damage as given by Eq. (19). The first part is due to the damage caused by excessive deformation and the second part is contribution of repeated cyclic loading effects to the damage.

$$D = \frac{\delta_m}{\delta_u} + \frac{\beta}{Q_y \delta_u} \int dE \quad (19)$$

where δ_m and δ_u are the maximum deformation under seismic loading and the ultimate deformation under monotonic load respectively. Since ultimate deformation under monotonic loading is not available, the value of δ_u is evaluated as post-peak deformation corresponding to 15% drop in peak load, as specified in EC8(2004). Q_y is the yield strength; dE is the incremental adsorbed hysteretic energy; Based on the regression analysis performed on the data of 402 reinforced concrete components of rectangular cross section which were tested till failure, Park and Ang (1987) suggested a value of 0.05 for β, for getting minimum variance solution for reinforced concrete component. However, Cosenza *et al*. (1993) and Karayannis and Golias (2018) reported that the damage index calculated using Park and Ang model with $\beta = 0.15$ correlates closely with the results of other models. Hence, $\beta = 0.15$ is adopted in present study. The damage indices for all the control (SP1, SP2, SP3) and retrofitted (SP1-R1, SP2-R1 and SP3-R1) specimens are evaluated using this parameter and compared in Fig.18.

The damage incurred by specimens are compared with reference to common damage index of 1.0. The evaluated damage index of the control GLD specimen SP1 is 1.0 at the drift ratio of 1.47%, whereas the damage index of retrofitted GLD specimen SP1-R1 reached a value of 1.0 at drift ratio of 2.2%. Furthermore, the damage index of control non-ductile specimen SP2 attained value of 1 at drift ratio of 2.2%. Whereas, the damage index of retrofitted non-ductile specimen SP2-R1 reached a value of around 1 at drift ratio of 2.94%. The damage index of control ductile specimen SP3 attained a damage index value of 1 at drift ratio of 2.94%. The retrofitted ductile specimen SP3-R1 attained a damage index value of 1 at drift ratio of 3.67%. Thus, the retrofitted specimens SP1-R1, SP2-R1 and SP3-R1 showed improved performance by delaying the damage. It could be observed that the damage indices of all the retrofitted specimens are lower when compared with their control undamaged counterparts, which demonstrates the efficacy of the retrofit adopted for earthquake damaged beam-column sub-assemblages.

7. Conclusions

Experimental investigations are carried out on beam-column sub-assemblages designed for three different levels, namely, i) Gravity load designed (SP1) (ii) seismic load designed without ductility detailing (SP2) and iii) Seismic load designed with ductility detailing (SP3), under reverse cyclic loading. These three types of specimens damaged under reverse cyclic loading, are then repaired and retrofitted using the innovative steel bracket and haunch hybrid retrofit solution proposed in this study. Furthermore, experimental investigations on repaired and retrofitted beam column sub-assemblages (SP1-R1, SP2-R1, SP3-R1) are carried out under reverse cyclic loading. The following conclusions are drawn from the experimental investigations carried out on undamaged control and retrofitted beam-column sub-assemblages of three different categories:

- The steel bracket and haunch hybrid retrofit adopted in SP1-R1 succeeded in preventing the anchorage failure of beam bottom reinforcement bars and this specimen could sustain higher drifts without any substantial reduction in load carrying capacity during the positive cycle of loading. During the negative cycle of loading, the retrofit delayed the shear failure of the joint and succeeded in transforming the failure from joint shear failure to beam flexural failure. The retrofit improved the load carrying capacity of the specimen SP1-R1 to the level of non-ductile specimen SP2 and qualifies the GLD specimen to the performance level of seismic load designed specimen.
- In the case of repaired and retrofitted specimen SP2-R1, the retrofit solution delayed the joint shear damage to the large extent and the specimen could sustain the peak load till the drift ratio greater than that of the control specimen SP2. Further, the retrofit succeeded in changing the failure pattern from joint shear failure to mixed mode of failure i.e. beam flexure and joint shear. The retrofit also succeeded in improving the performance of specimen SP2 to the desired displacement ductility level of three.
- In the case of the repaired and retrofitted ductile specimen (SP3-R1), the joint shear degradation is delayed. The retrofit could restore the load carrying capacity of damaged specimen to the level of undamaged specimen SP3 and also succeeded in achieving ductility closer to the desired displacement ductility of five.
- Double Steel bracket and haunch hybrid retrofit improved the ductility of all the repaired and retrofitted specimens tested, especially huge improvement in ductility is observed in the case of specimens SP1-R1 and SP2-R1.
- The retrofit improved the cumulative energy dissipation of the specimens to large extent. The repaired and retrofitted specimens SP1-R1, SP2-R1 and SP3-R1 dissipated nearly 6.5 times, 2.31 times and 1.21 times that of the corresponding control specimens SP1, SP2 and SP3 respectively.
- Equivalent viscous damping co-efficient values are found to be higher for retrofitted specimens when compared with the control specimens at all the drift ratios.
- The retrofitted specimens undergone lesser damage when compared with the control specimens. This could be witnessed in terms of lower damage indices of repaired and retrofitted specimens when compared with their undamaged control counterparts at any drift ratio.
- By adopting the innovative steel bracket and haunch hybrid retrofit, the challenging task of restoring the load carrying capacity of damaged beam-column sub-assemblage along with improved hysteretic performance could be achieved. The innovative steel bracket and haunch hybrid retrofit has demonstrated its effectiveness and efficacy i) by demonstrating the improved hysteretic behavior ii) by sustaining the peak load till higher drifts, iii) by favored damage progression and iv) by many fold increase in energy dissipation capacity. This innovative retrofit scheme would definitely be an excellent candidate for post-earthquake retrofit of damaged RC structures.

Acknowledgments

The authors express their heartfelt thanks to staff members of Advanced Concrete Testing and Evaluation Laboratory and Structural Testing Laboratory of CSIR-SERC for their support during the experimental investigations.

References

ACI 318M (2011), “Building Code Requirements for Structural Concrete and Commentary,” Farmington Hills, MI, U.S.A.

Adibi, M., Marefata, M.S., Arani, K.K. and Zare, H. (2017), "External retrofit of beam-column joints in old fashioned RC structures", *Earthq. Struct.*, **12**(2), 237-250. http://dx.doi.org/10.12989/eas.2017.12.2.237

Antonopoulos, C.P. and Triantafillou, T.C. (2003), "Experimental investigation of FRP-strengthened RC beam-column Joints", *J. Compos. Construct.*, **7**(1), 39-49. https://doi.org/10.1061/(ASCE)1090-0268(2003)7:1(39)

Balsamo, A., Colombo, A., Manfredi, G., Negro, P. and Prota A. (2005), "Seismic behaviour of a full-scale RC frame repaired using CFRP laminates", *Eng. Struct.,* **27,** 769-780. https://doi.org/10.1016/j.engstruct.2005.01.002

Bracci, J.M., Reinhorn, A.M. and Mander, J.B. (1995), "Seismic retrofit of reinforced concrete buildings designed for gravity loads: performance of structural model", *ACI Struct. J.*, **92**(6),711-723. https://doi.org/10.14359/9665

Campione, G., Cavaleri, L. and Papia, M. (2015), "Flexural response of external R.C. beam-column joints externally strengthened with steel cages", *Eng. Struct.*, **104**, 51-64. https://doi.org/10.1016/j.engstruct.2015.09.009

Chaimahawan, P. and Pimanmas, A. (2009), "Seismic retrofit of substandard beam-column joint by planar joint expansion", *Mater. Struct.*, **42,** 443-459. https://doi.org/10.1617/s11527-008-9393-7

Corte, G.D., Barecchia, E. and Mazzolani, F.M. (2006), "Seismic upgrading of RC buildings by FRP: Full-scale tests of a real Structure", *J. Mater. Civil Eng.*, **18**(5), 659-669. https://doi.org/10.1061/(ASCE)08991561(2006)18:5(659)

Cosenza, E., Manfredi, G. and Ramasco, R. (1993), "The use of damage functionals in earthquake engineering: a comparison between different methods", *Earthq. Eng. Struct. Dynam.*, **22**(10), pp.855-868. https://doi.org/10.1002/eqe.4290221003.

Duran, B., Tunaboyu, O., Atli, K.C. and Avşar, Ö. (2019), "Seismic performance upgrading of substandard RC frames using shape memory alloy bars", *Smart Mater. Struct.,* **28**, 085007 (21pp*). https://doi.org/10.1088/1361-665X/ab28f6*

EC8 (2004), Design of structures for earthquake resistance. Part 1: General rules, seismic actions and rules for buildings, European Committee for Standardization; Brussels, Belgium.

Elmenshawi, A., Brown, T. and El-Metwally, S. (2012), "Plastic hinge length considering shear reversal in reinforced concrete elements", *J. Earthq. Eng.*, **16**(2), pp.188-210. https://doi.org/10.1080/13632469.2011.597485

Garcia, R., Jemaa, Y., Helal, Y., Guadagnini, M. and Pilakoutas, K. (2014a), "Seismic strengthening of severely damaged beam-column RC joints using CFRP", *J. Compos. Construct.*, **18**(2), 04013048-1-10. https://doi.org/10.1061/(ASCE)CC.1943-5614.0000448

Garcia, R., Hajirasouliha, I., Guadagnini, M., Helal, Y., Jemaa, Y., Pilakoutas, K., *et al*, (2014b), "Full-Scale Shaking Table Tests on a Substandard RC Building Repaired and Strengthened with Post-Tensioned Metal Strap", *J. Earthq. Eng.*, **18,**187-213. https://doi.org/10.1080/13632469.2013.847874

Genesio, G. (2012), "Seismic Assessment of RC Exterior Beam-Column Joints and Retrofit with Haunches Using Post-Installed Anchors", Ph.D Dissertation; University of Stuttgart, Stuttgart, Germany.

Hwang, S.J. and Lee, H. J. (1999), "Analytical model for predicting shear strengths of exterior reinforced concrete beam-column joints for seismic resistance", *ACI Struct. J.*, **96**(5), 846-858. https://doi.org/10.14359/739

IS1893(2002), Criteria for earthquake resistant design of structures. Part 1: General provisions and buildings, Bureau of Indian Standards; New Delhi, India

IS456(2000), Code of practice for plain and reinforced concrete (Fourth revision), Bureau of Indian Standards; New Delhi, India.

IS13920(1993), Ductility detailing of reinforced concrete structures subjected to seismic forces; Bureau of Indian Standards, New Delhi, India.

Kakaletsis, D.J., David, K.N. and Karayannis, C.G. (2011) "Effectiveness of some conventional seismic retrofitting techniques for bare and infilled R/C frames", *Struct. Eng. Mech.*, **39**(4),499-520. http://dx.doi.org/10.12989/sem.2011.39.4.499.

Kalogeropoulos, G.I, Tsonos, A.G., Konstandinidis, D., and Tsetines, S. (2016), "Pre-earthquake and post-earthquake retrofitting of poorly detailed exterior RC beam-to-column joints", *Eng. Struct.*, **109**, 1-15. https://doi.org/10.1016/j.engstruct.2015.11.009.

Kanchanadevi, A., Ramanjaneyulu, K., Mayank, T. and Saptarshi S. (2018), "Novel non-invasive seismic upgradation strategies for gravity load designed exterior beam-column joints", *Arch. Civil Mech. Eng.*, **18,** 479- 489. https://doi.org/10.1016/j.acme.2017.08.005.

Kanchanadevi, A. and Ramanjaneyulu, K. (2018), "Non-invasive steel haunch upgradation strategy for seismically deficient reinforced concrete exterior beam-column sub-assemblages", *Steel Compos. Struct.*, **28**(6),719-734. http://dx.doi.org/10.12989/scs.2018.28.6.719

Kanchanadevi, A. and Ramanjaneyulu, K. (2019), "Non-invasive hybrid retrofit for seismic damage mitigation of gravity load designed exterior beam-column sub-assemblage", *J. Earthq. Eng.*, DOI:10.1080/13632469.2019.1592790.

Karayannis, C.G. and Sirkelis, G.M. (2008), "Strengthening and rehabilitation of RC beam–column joints using carbon-FRP jacketing and epoxy resin injection", *Earthq. Eng. Struct. Dynam.*, **37**,769-790. https://doi.org/10.1002/eqe.785

Karayannis, C.G. and Golias, E. (2018), "Full scale tests of RC joints with minor to moderate seismic damage repaired using C-FRP sheets", *Earthq. Struct.*, **15**(6), pp.617-627. https://doi.org/10.12989/eas.2018.15.6.617

Kheyroddin, A., Khalili, A., Emami, E. and Sharbatdar, M.K. (2016), "An innovative experimental method to upgrade performance of external weak RC joints using fused steel prop plus sheets", *Steel Compos. Struct.*, **21**(2), 443-460. http://dx.doi.org/10.12989/scs.2016.21.2.443

Li, Y. and Sanada, Y. (2017), "Seismic strengthening of existing RC beam-column joints by wing walls", *Earthq. Eng. Struct. Dynam.,* **46,** 1987–2008. https://doi.org/10.1002/eqe.2890

Mahrenholtz, C., Lin, P.C., Wu, A.C., Tsai, K.C., Hwang, S.J., Lin, R.Y. *et al*. (2015), "Retrofit of reinforced concrete frames with buckling-restrained braces", *Earthq. Eng. Struct. Dynam.*, **44**, 59-78. https://doi.org/10.1002/eqe.2458

Misir, I.S. and Kahraman, S. (2013), "Strengthening of non-seismically detailed reinforced concrete beam–column joints using SIFCON blocks", *Sadhana*, **38** (1), 69-88. https://doi.org/10.1007/s12046-013-0127-3

Mukherjee, A. and Joshi, M. (2005), "FRPC reinforced concrete beam-column joints under cyclic excitation", *Composite Structures*, **70**, 185-199. https://doi.org/10.1016/j.compstruct.2004.08.022

NZS 3101(2006), "Concrete Structures Standard Part 1 -The Design of Concrete Structures", Standards New Zealand, Wellington.

Pampanin, S., Christopoulos, C. and Chen, T.H. (2006), "Development and validation of a metallic haunch seismic retrofit solution for existing under-designed RC frame buildings", *Earthq. Eng. Struct. Dynam.*, **35,** 1739-1766. https://doi.org/10.1002/eqe.600

Park, Y. and Ang, A. (1985), "Mechanistic seismic damage model for reinforced-concrete", *J. Struct. Eng. ASCE*, **111**(4), 722-739. https://doi.org/10.1061/(ASCE)0733-9445(1985)111:4(722)

Park, Y.J., Ang, A.H.S. and Wen, Y. K. (1987), "Damage-limiting aseismic design of buildings", *Earthq. Spectra*, **3**(1), 1–26.

https://doi.org/10.1193/1.1585416

Paulay, T. and Priestley, M.N., 1992. Seismic design of reinforced concrete and masonry buildings.

Prota, A., Nanni, A., Manfredi, G. and Cosenza, E. (2003), "Capacity assessment of RC sub-assemblages upgraded with CFRP", *J. Reinforced Plastics Compos.*, **22**(14), 1287-1304. https://doi.org/10.1177/0731684403035580

Shafaei, J., Hosseini, A., Marefat, M.S. and Ingham, J.M. (2017), "Rehabilitation of earthquake damaged external RC beam-column joints by joint enlargement using prestressed steel angles", *Earthq. Eng. Struct. Dynam.,* **46,** 291-316. https://doi.org/10.1002/eqe.2794

Shannag, M.J., Barakat, S. and Abdul-Kareem M. (2002), "Cyclic behavior of HPFRC-repaired reinforced concrete interior beam-column joints", *Mater. Struct.,* **35,** 348-356. https://doi.org/10.1007/BF02483154

Shannag, M.J. and Alhassan, M.A. (2005), "Seismic upgrade of interior beam-column sub-assemblages with high-performance fiber-reinforced concrete jackets", *ACI Struct. J.*, **102**(1),131-138. https://doi.org/10.14359/13538

Sharma, A., Reddy, G.R., Eligehausen, R., Genesio, G. and Pampanin, S. (2014), "Seismic response of reinforced concrete frames with haunch retrofit solution", *ACI Struct. J.,* **111**(3), 673-684. https://doi.org/10.14359/51686625

Stoppenhagen, D.R., Jirsa, J.O. and Wyllie, L.A. (1995), "Seismic repair and strengthening of a severely damaged concrete frame", *ACI Struct. J.*, **92**(2),177-187. https://doi.org/10.14359/1157

Torabi, A. and Maheri, M.R. (2017), "Seismic repair and retrofit of RC beam–column joints using stiffened steel plates", *Iran. J. Sci. Technol. Transactions Civil. Eng.,* **41**(1),13-26. https://doi.org/10.1007/s40996-016-0027-y

Tsonos, A.G. (2008), "Effectiveness of CFRP-jackets and RC-jackets in post-earthquake and pre-earthquake retrofitting of beam–column sub-assemblages", *Eng. Struct.*, **30,** 777-793. https://doi.org/10.1016/j.engstruct.2007.05.008

Tsonos, A.G. (2014), "A new method for earthquake strengthening of old R/C structures without the use of conventional reinforcement", *Struct. Eng. Mech.*, **52**(2), 391-403. https://doi.org/10.12989/sem.2014.52.2.391

Wang, B., Zhu, S., Xu, Y.L. and Jiang, H. (2018), "Seismic Retrofitting of Non-Seismically Designed RC Beam-Column Joints using Buckling Restrained Haunches: Design and Analysis", *J. Earthq. Eng.*, **22**(7), 1188-1208. https://doi.org/10.1080/13632469.2016.1277441

Yang, Y., Chen, Y., Chen, Z., Wang, N. and Yud, Y. (2018), "Experimental study on seismic behavior of RC beam-column joints retrofitted using prestressed steel strips", *Earthq. Struct.*, **15**(5), 499-511. http://dx.doi.org/10.12989/eas.2018.15.5.499

Yu, Q.S., Uang, C.M. and Gross, J. (2000), "Seismic rehabilitation design of steel moment connection with welded haunch", *ASCE J. Struct. Eng.,* **126**(1), 69-78. https://doi.org/10.1061/(ASCE)0733-9445(2000)126:1(69)

Yurdakul, O. and Avsar, O. (2015), "Structural repairing of damaged reinforced concrete beam-column assemblies with CFRPs", *Struct. Eng. Mech.*, **54**(3), 521-543. https://doi.org/10.12989/sem.2015.54.3.521

Yurdakul, O. and Avsar, O. (2016), "Strengthening of substandard reinforced concrete beam-column joints by external post-tension rods", *Eng. Struct.*, **107,** 9-22. https://doi.org/10.1016/j.engstruct.2015.11.004

Yurdakul, Ö., Tunaboyu, O. and Avşar, Ö. (2018), "Retrofit of non-seismically designed beam-column joints by post-tensioned superelastic shape memory alloy bars", *Bulletin Earthq. Eng.*, **16**(11), pp.5279-5307. https://doi.org/10.1007/s10518-018-0323-y.

Zabihi, A., Tsang, H.H., Gad, E.F. and Wilson, J.L. (2018), "Seismic retrofit of exterior RC beam-column joint using diagonal haunch", *Eng. Struct.*, **174,** 753-767. https://doi.org/10.1016/j.engstruct.2018.07.100

CC